Search for the leptonic decays $D^{*+} \to e^+\nu_e$ and $D^{*+} \to \mu^+\nu_\mu$

M. Ablikim,[1] M. N. Achasov,[12,b] P. Adlarson,[72] M. Albrecht,[4] R. Aliberti,[33] A. Amoroso,[71a,71c] M. R. An,[37] Q. An,[68,55] Y. Bai,[54] O. Bakina,[34] R. Baldini Ferroli,[27a] I. Balossino,[28a] Y. Ban,[44,g] V. Batozskaya,[1,42] D. Becker,[33] K. Begzsuren,[30] N. Berger,[33] M. Bertani,[27a] D. Bettoni,[28a] F. Bianchi,[71a,71c] E. Bianco,[71a,71c] J. Bloms,[65] A. Bortone,[71a,71c] I. Boyko,[34] R. A. Briere,[5] A. Brueggemann,[65] H. Cai,[73] X. Cai,[1,55] A. Calcaterra,[27a] G. F. Cao,[1,60] N. Cao,[1,60] S. A. Cetin,[59a] J. F. Chang,[1,55] W. L. Chang,[1,60] G. R. Che,[41] G. Chelkov,[34,a] C. Chen,[41] Chao Chen,[52] G. Chen,[1] H. S. Chen,[1,60] M. L. Chen,[1,55,60] S. J. Chen,[40] S. M. Chen,[58] T. Chen,[1,60] X. R. Chen,[29,60] X. T. Chen,[1,60] Y. B. Chen,[1,55] Z. J. Chen,[24,h] W. S. Cheng,[71c] S. K. Choi,[52] X. Chu,[41] G. Cibinetto,[28a] F. Cossio,[71c] J. J. Cui,[47] H. L. Dai,[1,55] J. P. Dai,[76] A. Dbeyssi,[18] R. E. de Boer,[4] D. Dedovich,[34] Z. Y. Deng,[1] A. Denig,[33] I. Denysenko,[34] M. Destefanis,[71a,71c] F. De Mori,[71a,71c] Y. Ding,[38] Y. Ding,[32] J. Dong,[1,55] L. Y. Dong,[1,60] M. Y. Dong,[1,55,60] X. Dong,[73] S. X. Du,[78] Z. H. Duan,[40] P. Egorov,[34,a] Y. L. Fan,[73] J. Fang,[1,55] S. S. Fang,[1,60] W. X. Fang,[1] Y. Fang,[1] R. Farinelli,[28a] L. Fava,[71b,71c] F. Feldbauer,[4] G. Felici,[27a] C. Q. Feng,[68,55] J. H. Feng,[56] K. Fischer,[66] M. Fritsch,[4] C. Fritzsch,[65] C. D. Fu,[1] H. Gao,[60] Y. N. Gao,[44,g] Yang Gao,[68,55] S. Garbolino,[71c] I. Garzia,[28a,28b] P. T. Ge,[73] Z. W. Ge,[40] C. Geng,[56] E. M. Gersabeck,[64] A. Gilman,[66] K. Goetzen,[13] L. Gong,[38] W. X. Gong,[1,55] W. Gradl,[33] M. Greco,[71a,71c] L. M. Gu,[40] M. H. Gu,[1,55] Y. T. Gu,[15] C. Y. Guan,[1,60] A. Q. Guo,[29,60] L. B. Guo,[39] R. P. Guo,[46] Y. P. Guo,[11,f] A. Guskov,[34,a] W. Y. Han,[37] X. Q. Hao,[19] F. A. Harris,[62] K. K. He,[52] K. L. He,[1,60] F. H. Heinsius,[4] C. H. Heinz,[33] Y. K. Heng,[1,55,60] C. Herold,[57] G. Y. Hou,[1,60] Y. R. Hou,[60] Z. L. Hou,[1] H. M. Hu,[1,60] J. F. Hu,[53,i] T. Hu,[1,55,60] Y. Hu,[1] G. S. Huang,[68,55] K. X. Huang,[56] L. Q. Huang,[29,60] X. T. Huang,[47] Y. P. Huang,[1] Z. Huang,[44,g] Z. C. Huang,[41] T. Hussain,[70] N. Hüsken,[26,33] W. Imoehl,[26] M. Irshad,[68,55] J. Jackson,[26] S. Jaeger,[4] S. Janchiv,[30] E. Jang,[52] J. H. Jeong,[52] Q. Ji,[1] Q. P. Ji,[19] X. B. Ji,[1,60] X. L. Ji,[1,55] Y. Y. Ji,[47] Z. K. Jia,[68,55] P. C. Jiang,[44,g] S. S. Jiang,[37] X. S. Jiang,[1,55,60] Y. Jiang,[60] J. B. Jiao,[47] Z. Jiao,[22] S. Jin,[40] Y. Jin,[63] M. Q. Jing,[1,60] T. Johansson,[72] S. Kabana,[31] N. Kalantar-Nayestanaki,[61] X. L. Kang,[9] X. S. Kang,[38] R. Kappert,[61] M. Kavatsyuk,[61] B. C. Ke,[78] I. K. Keshk,[4] A. Khoukaz,[65] R. Kiuchi,[1] R. Kliemt,[13] L. Koch,[35] O. B. Kolcu,[59a] B. Kopf,[4] M. Kuemmel,[4] M. Kuessner,[4] A. Kupsc,[42,72] W. Kühn,[35] J. J. Lane,[64] J. S. Lange,[35] P. Larin,[18] A. Lavania,[25] L. Lavezzi,[71a,71c] T. T. Lei,[68,k] Z. H. Lei,[68,55] H. Leithoff,[33] M. Lellmann,[33] T. Lenz,[33] C. Li,[45] C. Li,[41] C. H. Li,[37] Cheng Li,[68,55] D. M. Li,[78] F. Li,[1,55] G. Li,[1] H. Li,[68,55] H. B. Li,[1,60] H. J. Li,[19] H. N. Li,[53,i] Hui Li,[41] J. Q. Li,[4] J. S. Li,[56] J. W. Li,[47] Ke Li,[1] L. J. Li,[1,60] L. K. Li,[1] Lei Li,[3] M. H. Li,[41] P. R. Li,[36,j,k] S. X. Li,[11] S. Y. Li,[58] T. Li,[47] W. D. Li,[1,60] W. G. Li,[1] X. H. Li,[68,55] X. L. Li,[47] Xiaoyu Li,[1,60] Y. G. Li,[44,g] Z. X. Li,[15] Z. Y. Li,[56] C. Liang,[40] H. Liang,[32] H. Liang,[1,60] H. Liang,[68,55] Y. F. Liang,[51] Y. T. Liang,[29,60] G. R. Liao,[14] L. Z. Liao,[47] J. Libby,[25] A. Limphirat,[57] C. X. Lin,[56] D. X. Lin,[29,60] T. Lin,[1] B. J. Liu,[1] C. Liu,[32] C. X. Liu,[1] D. Liu,[18,68] F. H. Liu,[50] Fang Liu,[1] Feng Liu,[6] G. M. Liu,[53,i] H. Liu,[36,j,k] H. B. Liu,[15] H. M. Liu,[1,60] Huanhuan Liu,[1] Huihui Liu,[20] J. B. Liu,[68,55] J. L. Liu,[69] J. Y. Liu,[1,60] K. Liu,[1] K. Y. Liu,[38] Ke Liu,[21] L. Liu,[68,55] Lu Liu,[41] M. H. Liu,[11,f] P. L. Liu,[1] Q. Liu,[60] S. B. Liu,[68,55] T. Liu,[11,f] W. K. Liu,[41] W. M. Liu,[68,55] X. Liu,[36,j,k] Y. Liu,[36,j,k] Y. B. Liu,[41] Z. A. Liu,[1,55,60] Z. Q. Liu,[47] X. C. Lou,[1,55,60] F. X. Lu,[56] H. J. Lu,[22] J. G. Lu,[1,55] X. L. Lu,[1] Y. Lu,[7] Y. P. Lu,[1,55] Z. H. Lu,[1,60] C. L. Luo,[39] M. X. Luo,[77] T. Luo,[11,f] X. L. Luo,[1,55] X. R. Lyu,[60] Y. F. Lyu,[41] F. C. Ma,[38] H. L. Ma,[1] L. L. Ma,[47] M. M. Ma,[1,60] Q. M. Ma,[1] R. Q. Ma,[1,60] R. T. Ma,[60] X. Y. Ma,[1,55] Y. Ma,[44,g] F. E. Maas,[18] M. Maggiora,[71a,71c] S. Maldaner,[4] S. Malde,[66] Q. A. Malik,[70] A. Mangoni,[27b] Y. J. Mao,[44,g] Z. P. Mao,[1] S. Marcello,[71a,71c] Z. X. Meng,[63] J. G. Messchendorp,[13,61] G. Mezzadri,[28a] H. Miao,[1,60] T. J. Min,[40] R. E. Mitchell,[26] X. H. Mo,[1,55,60] N. Yu. Muchnoi,[12,b] Y. Nefedov,[34] F. Nerling,[18,d] I. B. Nikolaev,[12,b] Z. Ning,[1,55] S. Nisar,[10,l] Y. Niu,[47] S. L. Olsen,[60] Q. Ouyang,[1,55,60] S. Pacetti,[27b,27c] X. Pan,[52] Y. Pan,[54] A. Pathak,[32] Y. P. Pei,[68,55] M. Pelizaeus,[4] H. P. Peng,[68,55] K. Peters,[13,d] J. L. Ping,[39] R. G. Ping,[1,60] S. Plura,[33] S. Pogodin,[34] V. Prasad,[68,55] F. Z. Qi,[1] H. Qi,[68,55] H. R. Qi,[58] M. Qi,[40] T. Y. Qi,[11,f] S. Qian,[1,55] W. B. Qian,[60] Z. Qian,[56] C. F. Qiao,[60] J. J. Qin,[69] L. Q. Qin,[14] X. P. Qin,[11,f] X. S. Qin,[47] Z. H. Qin,[1,55] J. F. Qiu,[1] S. Q. Qu,[58] K. H. Rashid,[70] C. F. Redmer,[33] K. J. Ren,[37] A. Rivetti,[71c] V. Rodin,[61] M. Rolo,[71c] G. Rong,[1,60] Ch. Rosner,[18] S. N. Ruan,[41] A. Sarantsev,[34,c] Y. Schelhaas,[33] C. Schnier,[4] K. Schoenning,[72] M. Scodeggio,[28a,28b] K. Y. Shan,[11,f] W. Shan,[23] X. Y. Shan,[68,55] J. F. Shangguan,[52] L. G. Shao,[1,60] M. Shao,[68,55] C. P. Shen,[11,f] H. F. Shen,[1,60] W. H. Shen,[60] X. Y. Shen,[1,60] B. A. Shi,[60] H. C. Shi,[68,55] J. Y. Shi,[1] q. q. Shi,[52] R. S. Shi,[1,60] X. Shi,[1,55] J. J. Song,[19] W. M. Song,[32,1] Y. X. Song,[44,g] S. Sosio,[71a,71c] S. Spataro,[71a,71c] F. Stieler,[33] P. P. Su,[52] Y. J. Su,[60] G. X. Sun,[1] H. Sun,[60] H. K. Sun,[1] J. F. Sun,[19] L. Sun,[73] S. S. Sun,[1,60] T. Sun,[1,60] W. Y. Sun,[32] Y. J. Sun,[68,55] Y. Z. Sun,[1] Z. T. Sun,[47] Y. X. Tan,[68,55] C. J. Tang,[51] G. Y. Tang,[1] J. Tang,[56] L. Y. Tao,[69] Q. T. Tao,[24,h] M. Tat,[66] J. X. Teng,[68,55] V. Thoren,[72] W. H. Tian,[49] Y. Tian,[29,60] I. Uman,[59b] B. Wang,[68,55] B. Wang,[1] B. L. Wang,[60] C. W. Wang,[40] D. Y. Wang,[44,g] F. Wang,[69] H. J. Wang,[36,j,k] H. P. Wang,[1,60] K. Wang,[1,55] L. L. Wang,[1] M. Wang,[47] Meng Wang,[1,60] S. Wang,[14] S. Wang,[11,f] T. Wang,[11,f] T. J. Wang,[41] W. Wang,[56] W. H. Wang,[73] W. P. Wang,[68,55] X. Wang,[44,g] X. F. Wang,[36,j,k] X. L. Wang,[11,f] Y. Wang,[58] Y. D. Wang,[43] Y. F. Wang,[1,55,60] Y. H. Wang,[45] Y. Q. Wang,[1] Yaqian Wang,[17,1] Z. Wang,[1,55] Z. Y. Wang,[1,60] Ziyi Wang,[60] D. H. Wei,[14] F. Weidner,[65] S. P. Wen,[1] D. J. White,[64] U. Wiedner,[4] G. Wilkinson,[66] M. Wolke,[72] L. Wollenberg,[4] J. F. Wu,[1,60] L. H. Wu,[1] L. J. Wu,[1,60] X. Wu,[11,f] X. H. Wu,[32] Y. Wu,[68] Y. J. Wu,[29] Z. Wu,[1,55] L. Xia,[68,55]

T. Xiang,[44,g] D. Xiao,[36,j,k] G. Y. Xiao,[40] H. Xiao,[11,f] S. Y. Xiao,[1] Y. L. Xiao,[11,f] Z. J. Xiao,[39] C. Xie,[40] X. H. Xie,[44,g] Y. Xie,[47] Y. G. Xie,[1,55] Y. H. Xie,[6] Z. P. Xie,[68,55] T. Y. Xing,[1,60] C. F. Xu,[1,60] C. J. Xu,[56] G. F. Xu,[1] H. Y. Xu,[63] Q. J. Xu,[16] X. P. Xu,[52] Y. C. Xu,[75] Z. P. Xu,[40] F. Yan,[11,f] L. Yan,[11,f] W. B. Yan,[68,55] W. C. Yan,[78] H. J. Yang,[48,e] H. L. Yang,[32] H. X. Yang,[1] Tao Yang,[1] Y. F. Yang,[41] Y. X. Yang,[1,60] Yifan Yang,[1,60] M. Ye,[1,55] M. H. Ye,[8] J. H. Yin,[1] Z. Y. You,[56] B. X. Yu,[1,55,60] C. X. Yu,[41] G. Yu,[1,60] T. Yu,[69] X. D. Yu,[44,g] C. Z. Yuan,[1,60] L. Yuan,[2] S. C. Yuan,[1] X. Q. Yuan,[1] Y. Yuan,[1,60] Z. Y. Yuan,[56] C. X. Yue,[37] A. A. Zafar,[70] F. R. Zeng,[47] X. Zeng,[6] Y. Zeng,[24,h] X. Y. Zhai,[32] Y. H. Zhan,[56] A. Q. Zhang,[1,60] B. L. Zhang,[1,60] B. X. Zhang,[1] D. H. Zhang,[41] G. Y. Zhang,[19] H. Zhang,[68] H. H. Zhang,[56] H. H. Zhang,[32] H. Q. Zhang,[1,55,60] H. Y. Zhang,[1,55] J. J. Zhang,[49] J. L. Zhang,[74] J. Q. Zhang,[39] J. W. Zhang,[1,55,60] J. X. Zhang,[36,j,k] J. Y. Zhang,[1] J. Z. Zhang,[1,60] Jianyu Zhang,[1,60] Jiawei Zhang,[1,60] L. M. Zhang,[58] L. Q. Zhang,[56] Lei Zhang,[40] P. Zhang,[1] Q. Y. Zhang,[37,78] Shuihan Zhang,[1,60] Shulei Zhang,[24,h] X. D. Zhang,[43] X. M. Zhang,[1] X. Y. Zhang,[47] X. Y. Zhang,[52] Y. Zhang,[66] Y. T. Zhang,[78] Y. H. Zhang,[1,55] Yan Zhang,[68,55] Yao Zhang,[1] Z. H. Zhang,[1] Z. L. Zhang,[32] Z. Y. Zhang,[73] Z. Y. Zhang,[41] G. Zhao,[1] J. Zhao,[37] J. Y. Zhao,[1,60] J. Z. Zhao,[1,55] Lei Zhao,[68,55] Ling Zhao,[1] M. G. Zhao,[41] S. J. Zhao,[78] Y. B. Zhao,[1,55] Y. X. Zhao,[29,60] Z. G. Zhao,[68,55] A. Zhemchugov,[34,a] B. Zheng,[69] J. P. Zheng,[1,55] Y. H. Zheng,[60] B. Zhong,[39] C. Zhong,[69] X. Zhong,[56] H. Zhou,[47] L. P. Zhou,[1,60] X. Zhou,[73] X. K. Zhou,[60] X. R. Zhou,[68,55] X. Y. Zhou,[37] Y. Z. Zhou,[11,f] J. Zhu,[41] K. Zhu,[1] K. J. Zhu,[1,55,60] L. X. Zhu,[60] S. H. Zhu,[67] S. Q. Zhu,[40] T. J. Zhu,[74] W. J. Zhu,[11,f] Y. C. Zhu,[68,55] Z. A. Zhu,[1,60] J. H. Zou,[1] and J. Zu[68,55]

(BESIII Collaboration)

[1]*Institute of High Energy Physics, Beijing 100049, People's Republic of China*
[2]*Beihang University, Beijing 100191, People's Republic of China*
[3]*Beijing Institute of Petrochemical Technology, Beijing 102617, People's Republic of China*
[4]*Bochum Ruhr-University, D-44780 Bochum, Germany*
[5]*Carnegie Mellon University, Pittsburgh, Pennsylvania 15213, USA*
[6]*Central China Normal University, Wuhan 430079, People's Republic of China*
[7]*Central South University, Changsha 410083, People's Republic of China*
[8]*China Center of Advanced Science and Technology, Beijing 100190, People's Republic of China*
[9]*China University of Geosciences, Wuhan 430074, People's Republic of China*
[10]*COMSATS University Islamabad, Lahore Campus, Defence Road, Off Raiwind Road, 54000 Lahore, Pakistan*
[11]*Fudan University, Shanghai 200433, People's Republic of China*
[12]*G.I. Budker Institute of Nuclear Physics SB RAS (BINP), Novosibirsk 630090, Russia*
[13]*GSI Helmholtzcentre for Heavy Ion Research GmbH, D-64291 Darmstadt, Germany*
[14]*Guangxi Normal University, Guilin 541004, People's Republic of China*
[15]*Guangxi University, Nanning 530004, People's Republic of China*
[16]*Hangzhou Normal University, Hangzhou 310036, People's Republic of China*
[17]*Hebei University, Baoding 071002, People's Republic of China*
[18]*Helmholtz Institute Mainz, Staudinger Weg 18, D-55099 Mainz, Germany*
[19]*Henan Normal University, Xinxiang 453007, People's Republic of China*
[20]*Henan University of Science and Technology, Luoyang 471003, People's Republic of China*
[21]*Henan University of Technology, Zhengzhou 450001, People's Republic of China*
[22]*Huangshan College, Huangshan 245000, People's Republic of China*
[23]*Hunan Normal University, Changsha 410081, People's Republic of China*
[24]*Hunan University, Changsha 410082, People's Republic of China*
[25]*Indian Institute of Technology Madras, Chennai 600036, India*
[26]*Indiana University, Bloomington, Indiana 47405, USA*
[27a]*INFN Laboratori Nazionali di Frascati, I-00044 Frascati, Italy*
[27b]*INFN Sezione di Perugia, I-06100 Perugia, Italy*
[27c]*University of Perugia, I-06100 Perugia, Italy*
[28a]*INFN Sezione di Ferrara, I-44122 Ferrara, Italy*
[28b]*University of Ferrara, I-44122 Ferrara, Italy*
[29]*Institute of Modern Physics, Lanzhou 730000, People's Republic of China*
[30]*Institute of Physics and Technology, Peace Avenue 54B, Ulaanbaatar 13330, Mongolia*
[31]*Instituto de Alta Investigación, Universidad de Tarapacá, Casilla 7D, Arica, Chile*
[32]*Jilin University, Changchun 130012, People's Republic of China*
[33]*Johannes Gutenberg University of Mainz, Johann-Joachim-Becher-Weg 45, D-55099 Mainz, Germany*
[34]*Joint Institute for Nuclear Research, 141980 Dubna, Moscow Region, Russia*

[35]*Justus-Liebig-Universitaet Giessen, II. Physikalisches Institut, Heinrich-Buff-Ring 16, D-35392 Giessen, Germany*
[36]*Lanzhou University, Lanzhou 730000, People's Republic of China*
[37]*Liaoning Normal University, Dalian 116029, People's Republic of China*
[38]*Liaoning University, Shenyang 110036, People's Republic of China*
[39]*Nanjing Normal University, Nanjing 210023, People's Republic of China*
[40]*Nanjing University, Nanjing 210093, People's Republic of China*
[41]*Nankai University, Tianjin 300071, People's Republic of China*
[42]*National Centre for Nuclear Research, Warsaw 02-093, Poland*
[43]*North China Electric Power University, Beijing 102206, People's Republic of China*
[44]*Peking University, Beijing 100871, People's Republic of China*
[45]*Qufu Normal University, Qufu 273165, People's Republic of China*
[46]*Shandong Normal University, Jinan 250014, People's Republic of China*
[47]*Shandong University, Jinan 250100, People's Republic of China*
[48]*Shanghai Jiao Tong University, Shanghai 200240, People's Republic of China*
[49]*Shanxi Normal University, Linfen 041004, People's Republic of China*
[50]*Shanxi University, Taiyuan 030006, People's Republic of China*
[51]*Sichuan University, Chengdu 610064, People's Republic of China*
[52]*Soochow University, Suzhou 215006, People's Republic of China*
[53]*South China Normal University, Guangzhou 510006, People's Republic of China*
[54]*Southeast University, Nanjing 211100, People's Republic of China*
[55]*State Key Laboratory of Particle Detection and Electronics, Beijing 100049, Hefei 230026, People's Republic of China*
[56]*Sun Yat-Sen University, Guangzhou 510275, People's Republic of China*
[57]*Suranaree University of Technology, University Avenue 111, Nakhon Ratchasima 30000, Thailand*
[58]*Tsinghua University, Beijing 100084, People's Republic of China*
[59a]*Turkish Accelerator Center Particle Factory Group, Istinye University, 34010, Istanbul, Turkey*
[59b]*Near East University, Nicosia, North Cyprus, Mersin 10, Turkey*
[60]*University of Chinese Academy of Sciences, Beijing 100049, People's Republic of China*
[61]*University of Groningen, NL-9747 AA Groningen, The Netherlands*
[62]*University of Hawaii, Honolulu, Hawaii 96822, USA*
[63]*University of Jinan, Jinan 250022, People's Republic of China*
[64]*University of Manchester, Oxford Road, Manchester, M13 9PL, United Kingdom*
[65]*University of Muenster, Wilhelm-Klemm-Strasse 9, 48149 Muenster, Germany*
[66]*University of Oxford, Keble Road, Oxford OX13RH, United Kingdom*
[67]*University of Science and Technology Liaoning, Anshan 114051, People's Republic of China*
[68]*University of Science and Technology of China, Hefei 230026, People's Republic of China*
[69]*University of South China, Hengyang 421001, People's Republic of China*
[70]*University of the Punjab, Lahore-54590, Pakistan*
[71a]*University of Turin and INFN, University of Turin, I-10125 Turin, Italy*
[71b]*University of Eastern Piedmont, I-15121 Alessandria, Italy*
[71c]*INFN, I-10125 Turin, Italy*
[72]*Uppsala University, Box 516, SE-75120 Uppsala, Sweden*
[73]*Wuhan University, Wuhan 430072, People's Republic of China*
[74]*Xinyang Normal University, Xinyang 464000, People's Republic of China*
[75]*Yantai University, Yantai 264005, People's Republic of China*
[76]*Yunnan University, Kunming 650500, People's Republic of China*
[77]*Zhejiang University, Hangzhou 310027, People's Republic of China*
[78]*Zhengzhou University, Zhengzhou 450001, People's Republic of China*

[a]Also at the Moscow Institute of Physics and Technology, Moscow 141700, Russia.
[b]Also at the Novosibirsk State University, Novosibirsk, 630090, Russia.
[c]Also at the NRC "Kurchatov Institute", PNPI, 188300, Gatchina, Russia.
[d]Also at Goethe University Frankfurt, 60323 Frankfurt am Main, Germany.
[e]Also at Key Laboratory for Particle Physics, Astrophysics and Cosmology, Ministry. of Education; Shanghai Key Laboratory for Particle Physics and Cosmology; Institute. of Nuclear and Particle Physics, Shanghai 200240, China.
[f]Also at Key Laboratory of Nuclear Physics and Ion-beam Application (MOE) and Institute of Modern Physics, Fudan University, Shanghai 200443, China.
[g]Also at State Key Laboratory of Nuclear Physics and Technology, Peking University, Beijing 100871, China.
[h]Also at School of Physics and Electronics, Hunan University, Changsha 410082, China.

(Received 15 May 2024; accepted 10 June 2024; published 9 July 2024)

We present the first search for the leptonic decays $D^{*+} \to e^+\nu_e$ and $D^{*+} \to \mu^+\nu_\mu$ by analyzing a data sample of electron-positron collisions recorded with the BESIII detector at center-of-mass energies between 4.178 and 4.226 GeV, corresponding to an integrated luminosity of 6.32 fb^{-1}. No significant signal is observed. The upper limits on the branching fractions for $D^{*+} \to e^+\nu_e$ and $D^{*+} \to \mu^+\nu_\mu$ are set to be 1.1×10^{-5} and 4.3×10^{-6} at 90% confidence level, respectively.

DOI: 10.1103/PhysRevD.110.012003

I. INTRODUCTION

Experimentally, the study of pure leptonic decays of ground-state charm mesons has entered the stage of precision measurement [1]. However, further exploration is needed for the pure leptonic decays of excited pseudoscalar mesons. The D^{*+} meson is the lightest excited state of the D^+ meson, whose quark content is $c\bar{d}$, with a spin equal to 1.

In the Standard Model (SM), the leptonic decays $D^{*+} \to \ell^+\nu_\ell$ ($\ell = e, \mu$) are described by the annihilation of the initial quark-antiquark pair into a virtual W^+ that materializes $\ell\nu_\ell$ pair as shown in Fig. 1. Throughout this paper, charge conjugation is always implied, unless explicitly specified otherwise.

The examination of $D^{*+} \to \ell^+\nu_\ell$ decays holds significance, as their decay rates are linked to the Cobibbo-Kobayashi-Maskawa (CKM) matrix elements. The decay width of $D^{*+} \to \ell^+\nu_\ell$ can be parametrized by the D^{*+} decay constant f_{D^*} [2,3] via

$$\Gamma = \frac{G_F^2}{12\pi}|V_{cd}|^2 f_{D^*}^2 m_{D^*}^3 \left(1 - \frac{m_\ell^2}{m_{D^*}^2}\right)^2 \left(1 + \frac{m_\ell^2}{2m_{D^*}^2}\right), \quad (1)$$

where G_F is the Fermi coupling constant, $|V_{cd}|$ is the CKM matrix element between the c and d quarks, and m_ℓ (m_{D^*}) is the mass of the lepton (D^{*+}). Several theoretical studies have anticipated the f_{D^*}, such as the nonrelativistic quark model, relativistic quark model, lattice QCD, etc., predicting f_{D^*} values between 186 and 391 MeV [4]. In addition, as the D^{*+} can decay by the strong interaction, the branching fractions of these weak decays are at the 10^{-10} level within the SM [3,5,6], but potential contributions from new pseudoscalar interactions beyond the SM could lift the branching fractions up to 10^{-5} [7–9]. Any observation of the leptonic D^{*+} decays at a rate above the SM prediction would be a potential hint of new physics.

This paper reports the first searches ever performed for the leptonic decays $D^{*+} \to e^+\nu_e$ and $D^{*+} \to \mu^+\nu_\mu$, using a data sample corresponding to an integrated luminosity of 6.32 fb^{-1}, recorded by the BESIII detector at center-of-mass (CM) energies ($\sqrt{s}$) ranging from 4.178 to 4.226 GeV.

II. DETECTOR AND DATASETS

The BESIII detector [10] records symmetric e^+e^- collisions provided by the BEPCII storage ring [11], which operates in $\sqrt{s}$ from 2.00 to 4.95 GeV, with a peak luminosity of 1×10^{33} cm^{-2} s^{-1} achieved at $\sqrt{s} = 3.77$ GeV. BESIII has collected large data samples in this energy region [12]. The cylindrical core of the BESIII detector covers 93% of the full solid angle and consists of a helium-based multilayer drift chamber (MDC), a plastic scintillator time-of-flight system (TOF), and a CsI(Tl) electromagnetic calorimeter (EMC), which are all enclosed in a superconducting solenoidal magnet providing a 1.0 T magnetic field. The solenoid is supported by an octagonal flux-return yoke with resistive plate counter muon identification modules interleaved with steel (MUC) [13]. The charged-particle momentum resolution at 1 GeV/c is 0.5%, and the specific ionization energy loss (dE/dx) resolution is 6% for electrons from Bhabha scattering. The EMC measures photon energies with a resolution of 2.5% (5%) at 1 GeV in the barrel (end cap)

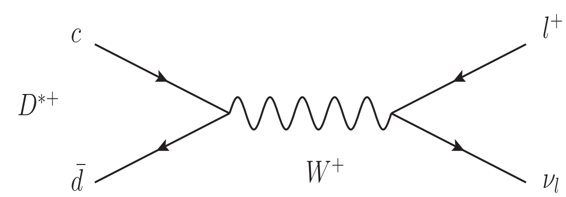

FIG. 1. Feynman diagram of $D^{*+} \to \ell^+\nu_\ell$.

[i]Also at Guangdong Provincial Key Laboratory of Nuclear Science, Institute of Quantum Matter, South China Normal University, Guangzhou 510006, China.
[j]Also at Frontiers Science Center for Rare Isotopes, Lanzhou University, Lanzhou 730000, China.
[k]Also at Lanzhou Center for Theoretical Physics, Lanzhou University, Lanzhou 730000, China.
[l]Also at the Department of Mathematical Sciences, IBA, Karachi, Pakistan.

TABLE I. Integrated luminosities $\mathcal{L}_{\rm int}$ [16,17] of the data samples at different energies. The first and second uncertainties are statistical and systematic, respectively.

$\sqrt{s}$ (GeV)	$\mathcal{L}_{\rm int}$ (pb^{-1})
4.178	$3189.0 \pm 0.2 \pm 31.9$
4.189	$526.7 \pm 0.1 \pm 2.2$
4.199	$526.0 \pm 0.1 \pm 2.1$
4.209	$517.1 \pm 0.1 \pm 1.8$
4.219	$514.6 \pm 0.1 \pm 1.8$
4.226	$1056.4 \pm 0.1 \pm 7.0$

region. The time resolution in the TOF barrel region is 68 ps, while that in the end cap region is 110 ps. The end cap TOF system was upgraded in 2015 using multigap resistive plate chamber technology, providing a time resolution of 60 ps [14].

The data samples used in this analysis are listed in Table I and provide a large sample of $D^{*\pm}$ mesons from $e^+e^- \to D^{*+}D^{*-}$ events with a cross section of about 3 nb [15].

Simulated Monte Carlo (MC) samples produced with GEANT4-based [18] software, which includes the geometric description of the BESIII detector and the detector response, are used to determine the detection efficiency and to estimate the background contributions. The simulation includes the beam-energy spread and initial-state radiation (ISR) in the e^+e^- annihilation modeled with the generator KKMC [19]. Inclusive MC samples of 40 times the size of the data samples are used to simulate the background contributions. The inclusive MC samples contain no signal decays and include the production of open-charm processes, the ISR production of vector charmonium(like) states, and the continuum processes incorporated in KKMC [19]. The known decay modes are modeled with EVTGEN [20] using world averaged branching fraction values [21], and the remaining unknown decays from the charmonium states are modeled with LUNDCHARM [22]. Final-state radiation from charged final-state particles is incorporated with PHOTOS [23].

III. DATA ANALYSIS

The single-tag (ST) sample comprises events in which only the D^{*-} meson is reconstructed via hadronic decay modes. The double-tag (DT) sample consists of events in which the leptonic decays of $D^{*+} \to \ell^+\nu_\ell$ are reconstructed in the systems recoiling against the ST candidates [24]. The branching fraction for $D^{*+} \to \ell^+\nu_\ell$ can be determined by

$$\mathcal{B}(D^{*+} \to \ell^+\nu_\ell) = \frac{N_{\rm DT}^{\rm cor}}{N_{\rm ST}^{\rm tot}}, \quad (2)$$

where $N_{\rm ST}^{\rm tot}$ is the ST yield in the data sample; $N_{\rm DT}^{\rm cor}$ is the DT yield in the data sample after efficiency correction, equal to $N_{\rm DT}^{\rm tot}/\bar{\epsilon}_{D^{*+}\to\ell^+\nu_\ell}$; and $\bar{\epsilon}_{D^{*+}\to\ell^+\nu_\ell} = \sum_i (N_{\rm ST}^i \epsilon_{\rm DT}^i / f\epsilon_{\rm ST}^i)/N_{\rm ST}^{\rm tot}$ is the effective averaged efficiency of reconstructing the $D^{*+} \to \ell^+\nu_\ell$ decay weighted by the ST yields, where i indicates the ith tag mode. Here, $\epsilon_{\rm ST}^i$ and $\epsilon_{\rm DT}^i$ are the efficiencies of reconstructing the ST and DT candidates in the ith tag mode (called the ST efficiency and DT efficiency, respectively). The ST efficiency is the average efficiency of ST D^{*-} from $D^{*+}D^{*-}$, $D^{*-}D^+$, $D^0D^{*-}\pi^+$, and $D^+D^{*-}\pi^0$. f represents the ratio of the number of D^{*-} contributed by all processes to that by $D^{*+}D^{*-}$ pairs, $f = (2\sigma_{D^{*-}D^{*+}} + \sigma_{D^{*-}D^+} + \sigma_{D^0D^{*-}\pi^+} + \sigma_{D^+D^{*-}\pi^0})/2\sigma_{D^{*+}D^{*-}}$, where the σ denotes the corresponding cross section [25,26]. Note that the cross section of $D^+D^{*-}\pi^0$ is set to be half of $D^0D^{*-}\pi^+$, according to the isospin symmetry.

A. Single-tag analysis

The ST candidates are reconstructed through the two main decay modes of D^{*-} mesons: $\bar{D}^0\pi^-$ and $D^-\pi^0$. To reconstruct $\bar{D}^0$ mesons, three hadronic decay modes, $K^+\pi^-$, $K^+\pi^-\pi^0$, and $K^+\pi^-\pi^+\pi^-$, are used. To reconstruct D^- mesons, six hadronic decay modes, $K^+\pi^-\pi^-$, $K^+K^-\pi^-$, $K^+\pi^-\pi^-\pi^0$, $K_S^0\pi^-$, $K_S^0\pi^-\pi^0$, and $K_S^0\pi^+\pi^-\pi^-$ are used.

All charged tracks are required to be within the polar angle (θ) range of $|\cos\theta| < 0.93$, where θ is defined with respect to the z axis, which is the symmetry axis of the MDC. For charged tracks not originating from K_S^0 decays, the distance of closest approach to the interaction point (IP) must be less than 10 cm along the z axis, $|V_z|$, and less than 1 cm in the transverse plane, $|V_{xy}|$. Particle identification (PID) for charged tracks combines measurements of the dE/dx and TOF to form likelihoods $\mathcal{L}(h)(h = K, \pi)$ for each hadron h hypothesis. Tracks are identified as charged kaons and pions by comparing the likelihoods for the kaon and pion hypotheses, $\mathcal{L}(K) > \mathcal{L}(\pi)$ and $\mathcal{L}(\pi) > \mathcal{L}(K)$, respectively.

Each K_S^0 candidate is reconstructed from two oppositely charged tracks satisfying $|V_z| < 20$ cm. The two charged tracks are assigned the charged pion hypothesis without imposing any PID requirements. The candidates pions are constrained to originate from a common vertex and are required to have an invariant mass within $|M_{\pi^+\pi^-} - m_{K_S^0}| < 12$ MeV$/c^2$, where $m_{K_S^0}$ is the known K_S^0 mass [21]. The decay length of the K_S^0 candidate is required to be twice greater than its uncertainty.

Photon candidates are identified using showers in the EMC. The deposited energy of each shower must be more than 25 MeV in the barrel region ($|\cos\theta| < 0.80$) and more than 50 MeV in the end cap region ($0.86 < |\cos\theta| < 0.92$). To exclude showers associated with charged tracks, the angle subtended by the EMC shower and the position of the closest charged track at the EMC must be greater than 10 deg as measured from the IP. To suppress electronic noise and showers unrelated to the event, the difference

TABLE II. ST selection requirements on ΔE, M_D, and $M_{\rm BC}$ for each tag mode.

Tag mode	ΔE (GeV)	M_D (GeV/c^2)	$M_{\rm BC}$ (GeV/c^2)
$\bar{D}^0 \to K^+\pi^-$	$(-0.024, 0.028)$	(1.846, 1.885)	(2.001, 2.024)
$\bar{D}^0 \to K^+\pi^-\pi^+\pi^-$	$(-0.024, 0.030)$	(1.850, 1.880)	(1.999, 2.025)
$\bar{D}^0 \to K^+\pi^-\pi^0$	$(-0.031, 0.047)$	(1.832, 1.890)	(1.994, 2.030)
$D^- \to K^+\pi^-\pi^-$	$(-0.025, 0.032)$	(1.854, 1.886)	(1.997, 2.029)
$D^- \to K^+K^-\pi^-$	$(-0.025, 0.032)$	(1.856, 1.884)	(2.000, 2.024)
$D^- \to K^+\pi^-\pi^-\pi^0$	$(-0.032, 0.046)$	(1.838, 1.893)	(1.998, 2.026)
$D^- \to K^0_S\pi^-$	$(-0.025, 0.028)$	(1.852, 1.890)	(1.998, 2.027)
$D^- \to K^0_S\pi^-\pi^0$	$(-0.036, 0.052)$	(1.831, 1.900)	(1.992, 2.033)
$D^- \to K^0_S\pi^-\pi^+\pi^-$	$(-0.027, 0.032)$	(1.852, 1.887)	(1.999, 2.025)

between the EMC time and the event start time is required to be within [0, 700] ns.

The π^0 candidates are reconstructed through $\pi^0 \to \gamma\gamma$ decays. The diphoton invariant masses $M_{\gamma\gamma}$ must lie within the range $[0.115, 0.150]$ GeV$/c^2$. For diphoton combinations satisfying this requirement $M_{\gamma\gamma}$ is kinematically constrained to the known π^0 mass [21].

If there are multiple ST candidates found, the candidate with the minimal $|\Delta E| \equiv |E_{D^{*-}} - E_{\rm beam}|$ is selected, where $E_{\rm beam}$ is the beam energy and $E_{D^{*-}}$ is the reconstructed energy of the ST candidate in the e^+e^- CM frame. Furthermore, it is possible that there are multiple combinations having exactly the same ΔE value for the ST modes with $\pi^-(\pi^0)$ as final states of $\bar{D}^0(D^-)$ decays. Specifically, in the case of $D^{*-} \to \pi^-\bar{D}^0(D^{*-} \to \pi^0 D^-)$ with $\bar{D}^0 \to X\pi^-(D^- \to X\pi^0)$, the value of ΔE remains unchanged even if the two $\pi^-(\pi^0)$ are switched. In this case, the least $|\Delta M| \equiv |M_{D^*} - m_{D^{-(0)}}|$ is used to identify the $\pi^{-(0)}$ meson produced from D^{*-} decays ($\pi^{-(0)}_{D^*}$) for further analysis. Here, M_{D^*} is the reconstructed mass of D^{*-} candidate, and $m_{D^{-(0)}}$ is the nominal mass of the $D^{-(0)}$ meson [21].

The $\pi^{-(0)}_{D^*}$ candidate is required to have momentum less than 100 MeV$/c$ to suppress backgrounds. Since the CM energies are about 160–210 MeV higher than the $D^{*+}D^{*-}$ mass threshold, the D^{*-} is boosted. MC studies show that more than 90% of signals have $\cos\theta_{D\pi} > 0$, where $\theta_{D\pi}$ is the opening angle between $D^{0(-)}$ and $\pi^{-(0)}_{D^*}$ in the e^+e^- CM frame. Therefore, a requirement of $\cos\theta_{D\pi} > 0$ is applied to suppress backgrounds caused by the misreconstruction of the $\pi^{-(0)}_{D^*}$.

The variables ΔE, the reconstructed mass of $\bar{D}^0(D^-)$ candidate (M_D), and the beam-constrained mass, $M_{\rm BC} = \sqrt{E^2_{\rm beam} - |\vec{p}_{D^{*-}}|^2}$, where $\vec{p}_{D^{*-}}$ is the reconstructed D^{*-} momentum in the e^+e^- CM frame, are used to further suppress combinatorial backgrounds. Requirements on these variables are listed in Table II, which correspond to 3σ regions for the signal process. Here, σ stands for the standard deviations for the variables that are determined by the fits on the corresponding distributions for each tag.

To determine the ST signal yield, a maximum-likelihood fit to the distributions of ΔM is performed for each tag mode at each energy point. In the fit, the signal shape is described by a double-Gaussian function and the background shape by a third-order polynomial. The ST yields ($N^i_{\rm ST}$), and efficiencies $\epsilon^i_{\rm ST}$ are extracted from the fits to data and inclusive MC samples, respectively. Signal regions of ΔM are set at three times the resolution. Figure 2 shows the fit results at 4.178 GeV, and Table III summarizes the signal regions of ΔM, ST signal yields, and ST efficiencies at 4.178 GeV. The fit results at other energy points can be found in Appendix A. These fits give a total ST yield of $N^{\rm tot}_{\rm ST} = 516256 \pm 1870$ at 4.178–4.226 GeV.

B. Double-tag analysis

To search for the $D^{*+} \to \ell^+\nu_\ell$ decays recoiling against ST candidates, we require that there is only one charged track (the number of extra charged tracks, $N^{\rm charge}_{\rm extra}$, is zero), which is identified as an e^+ or a μ^+, and the maximum energy of photon(s) not used in the ST candidate selection,

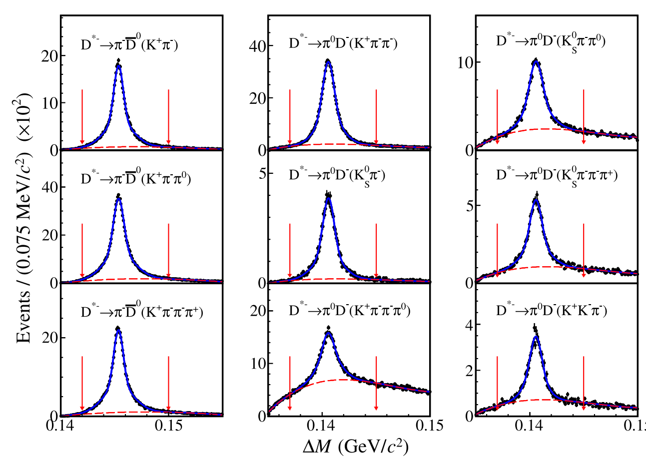

FIG. 2. Fits to the ΔM distributions of the accepted ST D^{*-} candidates at $\sqrt{s} = 4.178$ GeV. The points with error bars are data. The blue solid curves and red dashed curves represent the best fits and fitted combinatorial backgrounds, respectively. The pairs of red arrows indicate the ΔM signal region.

TABLE III. ST yields and efficiencies for each tag mode at 4.178 GeV. Uncertainties are statistical only.

Tag mode	ΔM (GeV/c^2)	$N^i_{\rm ST}$	$\epsilon^i_{\rm ST}$ (%)
$\bar{D}^0 \to K^+\pi^-$	(0.142, 0.150)	40325 ± 453	8.14 ± 0.04
$\bar{D}^0 \to K^+\pi^-\pi^+\pi^-$	(0.142, 0.150)	40325 ± 453	4.65 ± 0.02
$\bar{D}^0 \to K^+\pi^-\pi^0$	(0.142, 0.150)	86568 ± 888	4.86 ± 0.02
$D^- \to K^+\pi^-\pi^-$	(0.137, 0.145)	76303 ± 511	14.87 ± 0.05
$D^- \to K^+K^-\pi^-$	(0.137, 0.145)	6389 ± 241	11.66 ± 0.13
$D^- \to K^+\pi^-\pi^-\pi^0$	(0.137, 0.145)	24411 ± 648	6.68 ± 0.04
$D^- \to K^0_S\pi^-$	(0.137, 0.145)	9094 ± 193	14.85 ± 0.15
$D^- \to K^0_S\pi^-\pi^0$	(0.137, 0.145)	20942 ± 561	7.95 ± 0.05
$D^- \to K^0_S\pi^-\pi^+\pi^-$	(0.137, 0.145)	10922 ± 225	8.65 ± 0.08
Total		326405 ± 1567	

TABLE IV. Requirements of the hit depth in the MUC for muon candidate.

$\lvert\cos\theta\rvert$	p (GeV/c)	Depth (cm)
	$p \leq 0.88$	>17.0
(0.00, 0.20)	$0.88 < p < 1.04$	$>100.0 \times p - 71.0$
	$p \geq 1.04$	>33.0
	$p \leq 0.91$	>17.0
(0.20, 0.40)	$0.91 < p < 1.07$	$>100.0 \times p - 74.0$
	$p \geq 1.07$	>33.0
	$p \leq 0.94$	>17.0
(0.40, 0.60)	$0.94 < p < 1.10$	$>100.0 \times p - 77.0$
	$p \geq 1.10$	>33.0
(0.60, 0.80)	⋯	>17.0
(0.80, 0.93)	⋯	>17.0

$E^{\rm max}_{{\rm extra}\gamma}$, must be less than 0.3 GeV, to suppress backgrounds associated with photon(s).

Measurements in the MDC, TOF, and EMC are used to construct combined likelihoods ($\mathcal{L}'$) under the positron, pion, and kaon hypotheses. Positron candidates are required to satisfy $\mathcal{L}'(e) > 0.001$ and $\mathcal{L}'(e)/(\mathcal{L}'(e) + \mathcal{L}'(\pi) + \mathcal{L}'(K)) > 0.8$. To reduce background from hadrons and muons, the positron candidate is further required to have a deposited energy in the EMC greater than 80% of its momentum as determined from its trajectory in the MDC. Muon PID uses information from the EMC and MUC. The energy deposited in the EMC is required to be in the range of (0.0,0.3) GeV. The muon penetrates further than other charged particles and thus has a deeper hit depth in the MUC. The penetrating depths of muon candidates are required to satisfy the criteria listed in Table IV.

Neutrinos cannot be detected directly by the BESIII detector. However, their presence can be inferred in the process $e^+e^- \to D^{*+}D^{*-}$ by the kinematic variable $U_{\rm miss} = E_{\rm miss} - |\vec{p}_{\rm miss}|$, where $E_{\rm miss}$ is missing energy calculated by $E_{\rm miss} = E_{\rm cm} - E_{D^{*-}} - E_{\ell^+}$, and $\vec{p}_{\rm miss}$ is the momentum of the missing neutrino given by $\vec{p}_{\rm miss} = -\vec{p}_{D^{*-}} - \vec{p}_{\ell^+}$, where E_{ℓ^+} and $\vec{p}_{\ell^+}$ are the energy and momentum of e^+ or μ^+ in the e^+e^- CM frame,

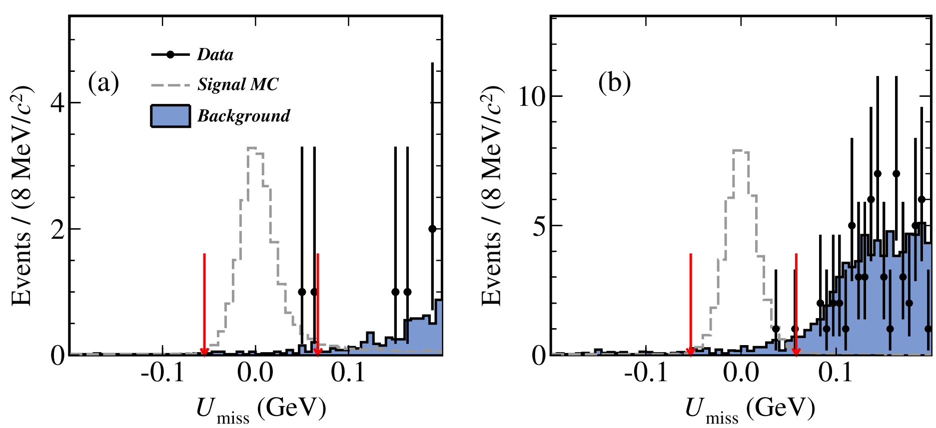

FIG. 3. The $U_{\rm miss}$ distributions for the (a) $D^{*+} \to e^+\nu_e$ and (b) $D^{*+} \to \mu^+\nu_\mu$ candidates. The points with error bars are data combined from all energy points. The blue filled histogram is the simulated background derived from the inclusive MC sample. The dashed histogram is the signal MC events with arbitrarily normalization for visualization. The signal region lies inside the red arrows, and the sideband region lies outside.

TABLE V. The DT efficiencies of $D^{*+} \to \ell^+\nu_\ell$ at 4.178 GeV. Uncertainties are statistical only.

Tag mode	$\epsilon^i_{\rm DT}$ (%)	
	$D^{*+} \to e^+\nu_e$	$D^{*+} \to \mu^+\nu_\mu$
$\bar{D}^0 \to K^+\pi^-$	6.90 ± 0.06	6.47 ± 0.06
$\bar{D}^0 \to K^+\pi^-\pi^+\pi^-$	3.87 ± 0.07	3.72 ± 0.07
$\bar{D}^0 \to K^+\pi^-\pi^0$	4.10 ± 0.05	3.91 ± 0.04
$D^- \to K^+\pi^-\pi^-$	17.38 ± 0.09	16.65 ± 0.09
$D^- \to K^+K^-\pi^-$	13.31 ± 0.11	12.75 ± 0.11
$D^- \to K^+\pi^-\pi^-\pi^0$	8.81 ± 0.09	8.27 ± 0.08
$D^- \to K^0_S\pi^-$	16.97 ± 0.11	16.08 ± 0.11
$D^- \to K^0_S\pi^-\pi^0$	9.37 ± 0.12	9.01 ± 0.12
$D^- \to K^0_S\pi^-\pi^+\pi^-$	9.88 ± 0.16	9.54 ± 0.16

respectively. A signal would manifest itself as an excess of events around $U_{\rm miss} = 0$. No significant signal is seen in the events passing the $D^{*+} \to \ell^+\nu_\ell$ selection, as can be seen in Fig. 3.

The $U_{\rm miss}$ signal and sideband regions are defined based on the signal MC events. Fits to signal MC events distributions are performed by using a double Gaussian function to model the signal shape and a third-order polynomial to model the background shape. The $U_{\rm miss}$ signal region is set to be three standard deviations around the fitted peaks, which correspond to $(-0.055, 0.067)$ GeV for $D^{*+} \to e^+\nu_e$ and $(-0.053, 0.058)$ GeV for $D^{*+} \to \mu^+\nu_\mu$. The sideband region for both selections is defined to be $U_{\rm miss}$ within $[-0.2, 0.2]$ GeV and lying outside the signal region.

The DT efficiencies for $D^{*+} \to \ell^+\nu_\ell$ events are calculated from the number of signal MC events falling into the signal regions divided by the number of generated signal MC events, in which D^{*+} decays to the $\ell^+\nu_\ell$ final state and D^{*-} decays to the tag modes. The DT efficiencies ($\epsilon^i_{\rm DT}$) for each tag mode at $\sqrt{s} = 4.178$ GeV are listed in Table V, and those for the other energy points can be found in Appendix B. From the DT efficiencies presented in this table and the ST efficiencies listed in Table III, the effective averaged efficiencies for reconstructing the $D^{*+} \to \ell^+\nu_\ell$ decay, $\bar{\epsilon}_{D^{*+}\to\ell^+\nu_\ell}$, are determined to be $(80.90 \pm 1.46)\%$ for $D^{*+} \to e^+\nu_e$ and $(68.86 \pm 1.23)\%$ for $D^{*+} \to \mu^+\nu_\mu$, after applying the muon PID systematic correction as described in Sec. V, where the uncertainties are statistical ones only.

From counting, we determine $N^{\rm data}_{\rm SR}$, the number of events in the $U_{\rm miss}$ signal region in data, and $N^{\rm data}_{\rm SB}$, the number in the data sideband region. The corresponding numbers in the inclusive MC sample are $N^{\rm MC}_{\rm SR}$ and $N^{\rm MC}_{\rm SB}$. We estimate the number of background events in the signal region to be $N^{\rm data}_{\rm SB}$ scaled by the factor $(N^{\rm MC}_{\rm SR}/N^{\rm MC}_{\rm SB})$. The number of events in each region for data and MC simulation is listed in Table VI.

IV. UPPER LIMITS OF BRANCHING FRACTIONS

Since there are only two and one events in the signal region for $D^{*+} \to e^+\nu_e$ and $D^{*+} \to \mu^+\nu_\mu$, respectively, the upper limits of their signal yields at the 90% confidence level, $N_{\rm UL}$, are calculated by using a frequentist method with an unbounded profile likelihood treatment of systematic uncertainties [27,28]. In this method, the numbers of signal and background events are assumed to follow a Poisson distribution, while the detection efficiency is assumed to obey Gaussian distribution, and the systematic uncertainty, as discussed later, is considered as the standard deviation of the efficiency. This is done by utilizing the TROLKE class [29] in the ROOT framework [30].

With the number of events in the $U_{\rm miss}$ signal region observed in data $N^{\rm data}_{\rm SR}$, the normalized number of events in the $U_{\rm miss}$ sideband region observed in data $N^{\rm data}_{\rm SB}$, the effective averaged efficiency $\bar{\epsilon}_{D^{*+}\to\ell^+\nu_\ell}$, the ratio of background events between the sideband and signal regions $\frac{N^{\rm MC}_{\rm SB}}{N^{\rm MC}_{\rm SR}}$, as well as the total systematic uncertainty $\delta_{\rm sys}$, the $N_{\rm UL}$ is calculated to be 5.9 for $D^{*+} \to e^+\nu_e$ and 2.2 for $D^{*+} \to \mu^+\nu_\mu$. Since the effective averaged efficiency $\bar{\epsilon}_{D^{*+}\to\ell^+\nu_\ell}$ has been considered in the determination of $N_{\rm UL}$ by the TROLKE package, the upper limits of the branching fractions are given by

$$\mathcal{B}_{\rm UL} = \frac{N_{\rm UL}}{N^{\rm tot}_{\rm ST}}. \qquad (3)$$

Finally, the upper limits of the branching fractions of $D^{*+} \to e^+\nu_e$ and $D^{*+} \to \mu^+\nu_\mu$ at 90% confidence level determined to be 1.1×10^{-5} and 4.1×10^{-6}, respectively, Table VI shows all quantities used for the branching fraction upper limit calculation and the obtained results.

V. SYSTEMATIC UNCERTAINTY

Table VII summarizes the assigned systematic uncertainties, which are discussed below.

The systematic uncertainties associated with $e^\pm(\mu^\pm)$ tracking and PID efficiencies are studied with a control

TABLE VI. The quantities used to calculate the branching fraction upper limits.

Signal mode	$N^{\rm tot}_{\rm ST}$	$N^{\rm data}_{\rm SR}$	$N^{\rm data}_{\rm SB}$	$N^{\rm MC}_{\rm SR}$	$N^{\rm MC}_{\rm SB}$	$\bar{\epsilon}_{D^{*+}\to\ell^+\nu_\ell}(\%)$	$N_{\rm UL}$	$\mathcal{B}_{\rm UL}$
$D^{*+} \to e^+\nu_e$	516256 ± 1870	2	4	34	239	80.90 ± 1.46	5.9	1.1×10^{-5}
$D^{*+} \to \mu^+\nu_\mu$		1	61	182	2872	68.86 ± 1.23	2.2	4.3×10^{-6}

TABLE VII. Relative systematic uncertainties (in %) from each source.

Source	$D^{*+} \to e^+\nu_e$	$D^{*+} \to \mu^+\nu_\mu$
Tracking	0.2	0.2
PID	0.5	0.5
$N_{\rm ST}^{\rm tot}$	2.9	2.9
$E_{\text{extra}\,\gamma}^{\max} < 0.3$ GeV	0.8	0.8
$N_{\rm extra}^{\rm charge} = 0$	0.2	0.2
Tag bias	0.7	0.8
f factor	4.1	4.1
MC sample sizes	1.0	1.0
Total	5.3	5.3

sample of $e^+e^- \to \gamma e^+e^-(\mu^+\mu^-)$ events. The efficiencies determined from this control sample are used to correct the efficiencies measured in the signal MC samples in the two dimensions of momentum and $\cos\theta$ and the difference in result taken as the corresponding systematic uncertainty for the tracking and electron PID efficiency. In the case of the muon PID, the systematic uncertainty is assigned by propagating the statistical uncertainty associated with the control sample to the branching-fraction measurement.

The uncertainty in the total number of ST D^{*-} mesons is assigned to be 2.9% by examining the changes in the fit yields when varying the signal and background shapes in the fit. The nominal signal shape is replaced with an MC-simulated shape convolved with a double-Gaussian function and the nominal background shape with an ARGUS function [31].

The uncertainties associated with the extra photon energy and extra charged track requirements are studied with samples of the light hadronic processes $e^+e^- \to K^+K^-\pi^+\pi^-, \pi^+\pi^-\pi^+\pi^-, K^+K^-\pi^+\pi^-\pi^0$, and $\pi^+\pi^-\pi^+\pi^-\pi^0$. The ratios of the average efficiencies of data to those of simulation are found to be 1.008 ± 0.001 for the extra photon-energy requirement and 0.998 ± 0.001 for the extra charged-track requirement. We assign 0.8% and 0.2% as the systematic uncertainties from the extra photon energy and charged track requirements, respectively.

The uncertainty associated with the ST efficiency does not fully cancel. Because the ST efficiencies estimated with the inclusive and signal MC samples differ from each other due to different multiplicities, there can be a bias associated with the reconstruction of the tag mode. We study the variation in tracking/PID efficiencies for different multiplicities and take the combined differences between data and MC simulation, 0.7% for $D^{*+} \to e^+\nu_e$ and 0.8% $D^{*+} \to \mu^+\nu_\mu$, as the corresponding tag-bias uncertainties. The efficiency for reconstructing the tag modes almost cancel with the DT method, and the residual effects are referred to as tag bias.

The systematic uncertainty caused by the change of f factor is estimated to be 4.1% as a result of cross section uncertainty of $D^{*+}D^{*-}$, $D^{*-}D^+$, $D^0D^{*-}\pi^+$, and $D^+D^{*-}\pi^0$, even including $D^{*0}D^{*-}\pi^+$ [32] and $D^{*+}D^{*-}\pi^0$. Similarly, according to the isospin symmetry, the cross section of $D^{*+}D^{*-}\pi^0$ is set to be half of $D^{*0}D^{*-}\pi^+$. The uncertainty in the knowledge of the ST and DT efficiencies arising from the limited MC sample sizes, as shown in Tables III and V, is evaluated to be 1.0% for each signal decay mode. Lastly, the total systematic uncertainty, $\delta_{\rm sys}$, is 5.3% for both $D^{*+} \to e^+\nu_e$ and $D^{*+} \to \mu^+\nu_\mu$.

VI. CONCLUSION

Using a data sample corresponding to an integrated luminosity of 6.32 fb^{-1}, taken at $\sqrt{s} = 4.178$–4.226 GeV by the BESIII detector, we search for the leptonic decays of $D^{*+} \to e^+\nu_e$ and $D^{*+} \to \mu^+\nu_\mu$ for the first time. No significant signal is observed. We set upper limits on the branching fractions of these decays, which are $\mathcal{B}(D^{*+} \to e^+\nu_e) < 1.1 \times 10^{-5}$ and $\mathcal{B}(D^{*+} \to \mu^+\nu_\mu) < 4.3 \times 10^{-6}$ at the 90% confidence level. The larger datasets that are foreseen to be collected at BESIII in the coming years [12] will offer the opportunity to further improve the sensitivity to these decays.

ACKNOWLEDGMENTS

The BESIII Collaboration thanks the staff of BEPCII and the IHEP computing center for their strong support. This work is supported in part by National Key R&D Program of China under Contracts No. 2020YFA0406300 and No. 2020YFA0406400; National Natural Science Foundation of China (NSFC) under Contracts No. 12035009, No. 123B2077, No. 11875170, No. 11875054, No. 11635010, No. 11735014, No. 11835012, No. 11935015, No. 11935016, No. 11935018, No. 11961141012, No. 12022510, No. 12025502, No. 12035013, No. 12192260, No. 12192261, No. 12192262, No. 12192263, No. 12192264, and No. 12192265; the Chinese Academy of Sciences (CAS) Large-Scale Scientific Facility Program; Joint Large-Scale Scientific Facility Funds of the NSFC and CAS under Contracts No. U1832207 and No. U2032104; the CAS Center for Excellence in Particle Physics (CCEPP); 100 Talents Program of CAS; The Excellent Youth Foundation of Henan Scientific Commitee under Contract No. 242300421044; the Institute of Nuclear and Particle Physics (INPAC) and Shanghai Key Laboratory for Particle Physics and Cosmology; ERC under Contract No. 758462; European Union's Horizon 2020 research and innovation programme under Marie Sklodowska-Curie grant agreement under Contract No. 894790; German Research Foundation DFG under Contracts No. 443159800 and No. 455635585; Collaborative Research Center Grants No. CRC 1044, No. FOR5327, and No. GRK 2149; Istituto Nazionale di Fisica Nucleare, Italy; Ministry of Development of Turkey under Contract No. DPT2006K-

120470; National Science and Technology fund; National Science Research and Innovation Fund (NSRF) via the Program Management Unit for Human Resources & Institutional Development, Research and Innovation under Contract No. B16F640076; Olle Engkvist Foundation under Contract No. 200-0605; STFC (United Kingdom); Suranaree University of Technology (SUT), Thailand Science Research and Innovation (TSRI), and National Science Research and Innovation Fund (NSRF) under Contract No. 160355; The Royal Society, United Kingdom, under Contracts No. DH140054 and No. DH160214; The Swedish Research Council; and U.S. Department of Energy under Contract No. DE-FG02-05ER41374.

APPENDIX A: ST YIELDS AND EFFICIENCIES

Tables VIII and IX summarize the ST efficiencies and the ST yields in data at $\sqrt{s} = 4.189$–4.226 GeV, respectively. Figures 4–8 show the fits to the ΔM distributions of the accepted ST D^{*-} candidates at these energy points.

TABLE VIII. ST efficiencies at $\sqrt{s} = 4.189$–4.226 GeV. The uncertainties are statistical only.

	ϵ^i_{ST} (%)				
Tag mode	4.189	4.199	4.209	4.219	4.226
$\bar{D}^0 \to K^-\pi^+$	8.66 ± 0.23	7.89 ± 0.17	8.15 ± 0.22	5.50 ± 0.17	5.33 ± 0.20
$\bar{D}^0 \to K^-\pi^+\pi^+\pi^-$	3.98 ± 0.11	4.73 ± 0.10	4.36 ± 0.10	3.30 ± 0.12	2.97 ± 0.08
$\bar{D}^0 \to K^-\pi^+\pi^0$	4.25 ± 0.10	4.86 ± 0.09	4.56 ± 0.09	3.62 ± 0.10	3.53 ± 0.33
$D^+ \to K^-\pi^+\pi^+$	12.28 ± 0.17	14.06 ± 0.23	13.13 ± 0.22	9.26 ± 0.23	8.38 ± 0.66
$D^+ \to K^+K^-\pi^+$	8.88 ± 2.43	10.28 ± 0.61	11.22 ± 1.48	6.71 ± 0.59	5.72 ± 0.55
$D^+ \to K^-\pi^+\pi^+\pi^0$	6.41 ± 0.44	6.73 ± 0.32	5.30 ± 0.31	5.65 ± 0.50	4.04 ± 0.29
$D^+ \to K^0_s\pi^+$	12.09 ± 0.56	13.09 ± 0.50	12.92 ± 0.72	9.45 ± 0.74	8.75 ± 0.98
$D^+ \to K^0_s\pi^+\pi^0$	7.44 ± 0.48	7.22 ± 0.30	6.59 ± 0.32	3.71 ± 0.23	4.12 ± 0.25
$D^+ \to K^0_s\pi^+\pi^+\pi^-$	7.67 ± 0.46	8.08 ± 0.37	8.27 ± 0.73	5.54 ± 0.66	3.91 ± 0.31

TABLE IX. ST yields in data at $\sqrt{s} = 4.189$–4.226 GeV. Uncertainties are statistical only.

	N^i_{ST}				
Tag mode	4.189	4.199	4.209	4.219	4.226
$\bar{D}^0 \to K^-\pi^+$	6070 ± 197	5546 ± 147	4264 ± 109	3644 ± 149	5402 ± 144
$\bar{D}^0 \to K^-\pi^+\pi^+\pi^-$	7626 ± 214	7444 ± 207	5511 ± 144	4632 ± 125	7243 ± 187
$\bar{D}^0 \to K^-\pi^+\pi^0$	13081 ± 342	12143 ± 443	10059 ± 232	8316 ± 309	12004 ± 262
$D^+ \to K^-\pi^+\pi^+$	10675 ± 210	9587 ± 308	7293 ± 210	5495 ± 177	8195 ± 142
$D^+ \to K^+K^-\pi^+$	938 ± 76	899 ± 85	560 ± 42	370 ± 126	645 ± 56
$D^+ \to K^-\pi^+\pi^+\pi^0$	3180 ± 313	1864 ± 212	2271 ± 147	1302 ± 206	2612 ± 256
$D^+ \to K^0_s\pi^+$	1120 ± 50	1151 ± 84	978 ± 80	546 ± 32	903 ± 128
$D^+ \to K^0_s\pi^+\pi^0$	2590 ± 121	2162 ± 82	1625 ± 79	1175 ± 69	2300 ± 152
$D^+ \to K^0_s\pi^+\pi^+\pi^-$	1664 ± 281	1234 ± 88	1097 ± 160	798 ± 78	951 ± 57
Sum	46944 ± 667	43123 ± 655	33251 ± 438	26278 ± 445	40255 ± 472

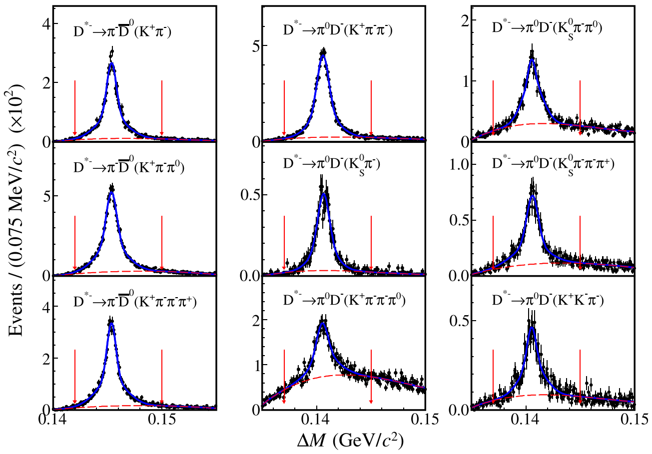

FIG. 4. Fits to the ΔM distributions of the accepted ST D^{*-} candidates at $\sqrt{s} = 4.189$ GeV. The points with error bars are data. The blue solid curves and red dashed curves represent the best fits and fitted combinatorial backgrounds, respectively. The pairs of red arrows indicate the ΔM signal region.

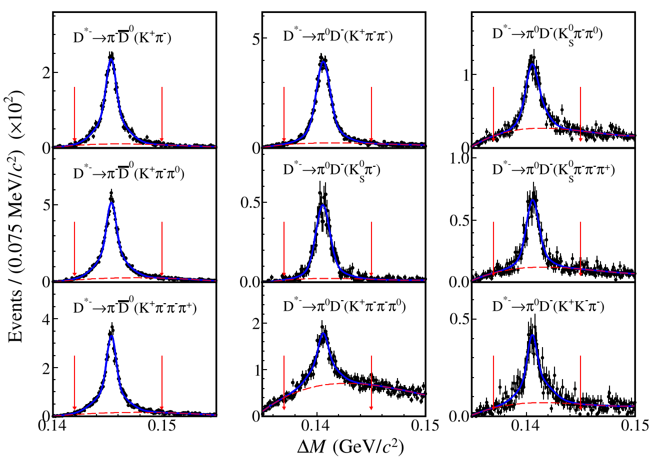

FIG. 5. Fits to the ΔM distributions of the accepted ST D^{*-} candidates at $\sqrt{s} = 4.199$ GeV. The points with error bars are data. The blue solid curves and red dashed curves represent the best fits and fitted combinatorial backgrounds, respectively. The pairs of red arrows indicate the ΔM signal region.

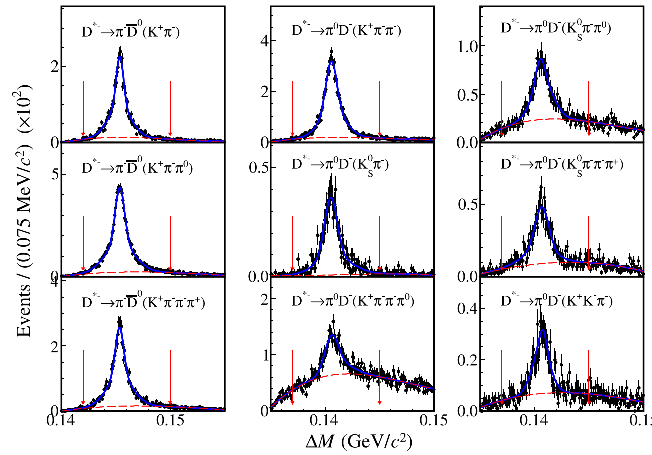

FIG. 6. Fits to the ΔM distributions of the accepted ST D^{*-} candidates at $\sqrt{s} = 4.209$ GeV. The points with error bars are data. The blue solid curves and red dashed curves represent the best fits and fitted combinatorial backgrounds, respectively. The pairs of red arrows indicate the ΔM signal region.

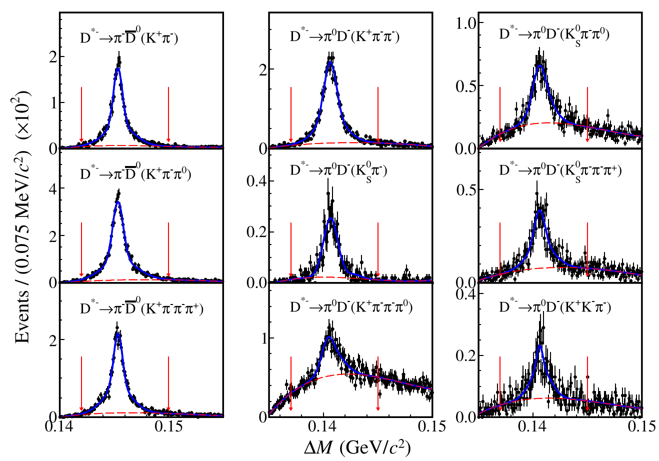

FIG. 7. Fits to the ΔM distributions of the accepted ST D^{*-} candidates at $\sqrt{s} = 4.219$ GeV. The points with error bars are data. The blue solid curves and red dashed curves represent the best fits and fitted combinatorial backgrounds, respectively. The pairs of red arrows indicate the ΔM signal region.

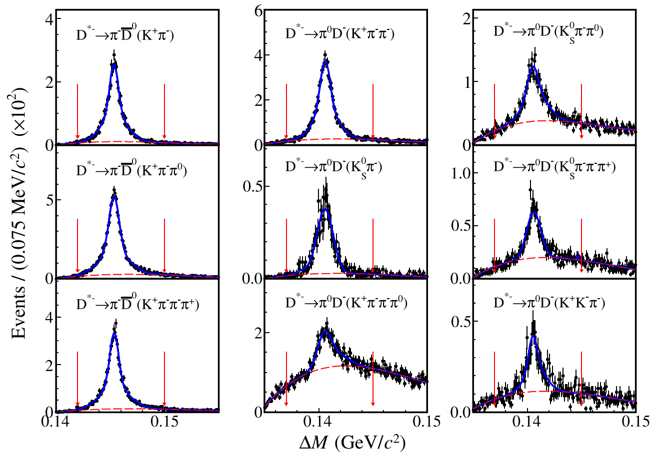

FIG. 8. Fits to the ΔM distributions of the accepted ST D^{*-} candidates at $\sqrt{s} = 4.226$ GeV. The points with error bars are data. The blue solid curves and red dashed curves represent the best fits and fitted combinatorial backgrounds, respectively. The pairs of red arrows indicate the ΔM signal region.

APPENDIX B: DT EFFICIENCIES

Tables X and XI summarize the DT efficiencies of $D^{*+} \to e^+\nu_e$ and $D^{*+} \to \mu^+\nu_\mu$ at $\sqrt{s} = 4.189$–4.226 GeV, respectively.

TABLE X. DT efficiencies of $D^{*+} \to e^+\nu_e$ at $\sqrt{s} = 4.189$–4.226 GeV.

	$\epsilon^i_{\mathrm{ST},D^{*+}\to e^+\nu_e}$				
Tag mode	4.189	4.199	4.209	4.219	4.226
$\bar{D}^0 \to K^-\pi^+$	7.20 ± 0.06	7.52 ± 0.06	6.99 ± 0.06	6.67 ± 0.06	6.50 ± 0.06
$\bar{D}^0 \to K^-\pi^+\pi^+\pi^-$	4.12 ± 0.07	4.29 ± 0.07	3.99 ± 0.07	3.91 ± 0.07	3.83 ± 0.07
$\bar{D}^0 \to K^-\pi^+\pi^0$	4.22 ± 0.05	4.39 ± 0.05	4.25 ± 0.05	4.05 ± 0.05	3.86 ± 0.04
$D^+ \to K^-\pi^+\pi^+$	17.34 ± 0.09	16.93 ± 0.09	15.68 ± 0.09	14.38 ± 0.08	12.66 ± 0.08
$D^+ \to K^+K^-\pi^+$	13.31 ± 0.11	13.11 ± 0.11	11.94 ± 0.10	11.01 ± 0.10	9.74 ± 0.09
$D^+ \to K^-\pi^+\pi^+\pi^0$	8.70 ± 0.08	8.65 ± 0.08	7.90 ± 0.08	7.28 ± 0.08	6.87 ± 0.08
$D^+ \to K^0_s\pi^+$	16.85 ± 0.09	16.59 ± 0.09	15.13 ± 0.09	13.76 ± 0.08	12.22 ± 0.08
$D^+ \to K^0_s\pi^+\pi^0$	9.20 ± 0.07	9.18 ± 0.07	8.46 ± 0.07	7.79 ± 0.06	7.12 ± 0.06
$D^+ \to K^0_s\pi^+\pi^+\pi^-$	8.38 ± 0.09	8.32 ± 0.09	7.77 ± 0.09	7.03 ± 0.08	6.69 ± 0.08

TABLE XI. DT efficiencies of $D^{*+} \to \mu^+\nu_\mu$ at $\sqrt{s} = 4.189$–4.226 GeV.

	$\epsilon^i_{\mathrm{ST},D^{*+}\to \mu^+\nu_\mu}$				
Tag mode	4.189	4.199	4.209	4.219	4.226
$\bar{D}^0 \to K^-\pi^+$	6.74 ± 0.06	7.00 ± 0.06	6.64 ± 0.06	6.27 ± 0.06	6.02 ± 0.05
$\bar{D}^0 \to K^-\pi^+\pi^+\pi^-$	3.90 ± 0.07	4.12 ± 0.07	4.00 ± 0.07	3.65 ± 0.07	3.59 ± 0.07
$\bar{D}^0 \to K^-\pi^+\pi^0$	3.87 ± 0.04	4.15 ± 0.05	3.93 ± 0.04	3.67 ± 0.04	3.57 ± 0.04
$D^+ \to K^-\pi^+\pi^+$	16.47 ± 0.09	16.03 ± 0.09	15.03 ± 0.09	13.49 ± 0.08	11.98 ± 0.08
$D^+ \to K^+K^-\pi^+$	12.49 ± 0.11	12.38 ± 0.11	11.54 ± 0.10	10.34 ± 0.10	9.15 ± 0.09
$D^+ \to K^-\pi^+\pi^+\pi^0$	8.23 ± 0.08	7.99 ± 0.08	7.42 ± 0.08	7.21 ± 0.08	6.36 ± 0.07
$D^+ \to K^0_s\pi^+$	16.12 ± 0.09	15.69 ± 0.09	14.54 ± 0.09	13.18 ± 0.08	11.69 ± 0.08
$D^+ \to K^0_s\pi^+\pi^0$	8.75 ± 0.07	8.69 ± 0.07	7.94 ± 0.06	7.30 ± 0.06	6.69 ± 0.06
$D^+ \to K^0_s\pi^+\pi^+\pi^-$	7.95 ± 0.09	7.96 ± 0.09	7.12 ± 0.08	6.73 ± 0.08	6.16 ± 0.08

[1] B. C. Ke, J. Koponen, H. B. Li, and Y. Zheng, Annu. Rev. Nucl. Part. Sci. **73**, 285 (2023).
[2] Z. G. Wang, Eur. Phys. J. C **75**, 427 (2015).
[3] Y. L. Yang, Z. L. Li, K. Li, J. S. Huang, and J. F. Sun, Eur. Phys. J. C **81**, 1110 (2021).
[4] K. Dash, P. C. Dash, R. N. Panda, S. Kar, and N. Barik, arxiv:2312.06130.
[5] N. Dhiman and H. Dahiya, Eur. Phys. J. Plus **133**, 134 (2017).
[6] K. Bowler, L. Del Debbio, J. M. Flynn, G. N. Lacagnina, V. I. Lesk, C. M. Maynard, and D. G. Richards (UKQCD Collaboration), Nucl. Phys. **B619**, 507 (2001).
[7] A. G. Akeroyd and F. Mahmoudi, J. High Energy Phys. 04 (2009) 121.
[8] A. G. Akeroyd and S. Recksiegel, Phys. Lett. B **554**, 38 (2003).
[9] A. G. Akeroyd, Prog. Theor. Phys. **111**, 295 (2004).
[10] M. Ablikim *et al.* (BESIII Collaboration), Nucl. Instrum. Methods Phys. Res., Sect. A **614**, 345 (2010).
[11] C. H. Yu *et al.*, *Proceedings of IPAC2016, Busan, Korea* (JACoW, Geneva, Switzerland, 2016), 10.18429/JACoW-IPAC2016-TUYA01.
[12] M. Ablikim *et al.* (BESIII Collaboration), Chin. Phys. C **44**, 040001 (2020).
[13] K. X. Huang *et al.*, Nucl. Sci. Tech. **33**, 142 (2022).
[14] X. Li *et al.*, Radiat. Detect. Technol. Methods **1**, 13 (2017); Y. X. Guo *et al.*, Radiat. Detect. Technol. Methods **1**, 15 (2017); P. Cao *et al.*, Nucl. Instrum. Methods Phys. Res., Sect. A **953**, 163053 (2020).
[15] K. Abe *et al.* (Belle Collaboration), Phys. Rev. Lett. **98**, 092001 (2007).
[16] M. Ablikim *et al.* (BESIII Collaboration), Chin. Phys. C **39**, 093001 (2015).
[17] M. Ablikim *et al.* (BESIII Collaboration), Chin. Phys. C **46**, 113002 (2022).
[18] S. Agostinelli *et al.* (GEANT4 Collaboration), Nucl. Instrum. Methods Phys. Res., Sect. A **506**, 250 (2003).
[19] S. Jadach, B. F. L. Ward, and Z. Was, Phys. Rev. D **63**, 113009 (2001).
[20] D. J. Lange, Nucl. Instrum. Methods Phys. Res., Sect. A **462**, 152 (2001); R. G. Ping, Chin. Phys. C **32**, 599 (2008).
[21] P. A. Zyla *et al.* (Particle Data Group), Prog. Theor. Exp. Phys. **2020**, 083C01 (2020) and 2021 update.
[22] J. C. Chen, G. S. Huang, X. R. Qi, D. H. Zhang, and Y. S. Zhu, Phys. Rev. D **62**, 034003 (2000); R. L. Yang, R. G. Ping, and H. Chen, Chin. Phys. Lett. **31**, 061301 (2014).
[23] E. Richter-Was, Phys. Lett. B **303**, 163 (1993).
[24] J. Adler *et al.* (MARK-III Collaboration), Phys. Rev. Lett. **62**, 1821 (1989).
[25] M. Ablikim *et al.* (BESIII Collaboration), J. High Energy Phys. 05 (2022) 155.
[26] M. Ablikim *et al.* (BESIII Collaboration), Phys. Rev. Lett. **122**, 102002 (2019).
[27] W. A. Rolke, A. M. Lopez, and J. Conrad, Nucl. Instrum. Methods Phys. Res., Sect. A **551**, 493 (2005).
[28] J. Lundberg, J. Conrad, W. Rolke, and A. Lopez, Comput. Phys. Commun. **181**, 683 (2010).
[29] https://root.cern.ch/doc/master/TRolke_8cxx_source.html#l01082
[30] http://root.cern.ch/
[31] H. Albrecht *et al.* (ARGUS Collaboration), Phys. Lett. B **241**, 278 (1990).
[32] M. Ablikim *et al.* (BESIII Collaboration), Phys. Rev. Lett. **130**, 121901 (2023).